International Journal of Solids and Structures 50 (2013) 1154–1163

Contents lists available at SciVerse ScienceDirect

International Journal of Solids and Structures

journal homepage: www.elsevier.com/locate/ijsolstr

Effective longitudinal shear moduli of periodic fibre-reinforced composites with functionally-graded fibre coatings

Edoardo Artioli *, Paolo Bisegna

Department of Civil Engineering and Computer Science, University of Rome "Tor Vergata", via del Politecnico 1, 00133 Rome, Italy

ARTICLE INFO

Article history:
Received 21 July 2012
Received in revised form 3 December 2012
Available online 4 January 2013

Keywords:
Micromechanics
Fibre-reinforced composite materials
Functionally graded coating
Effective moduli
Asymptotic homogenization
Analytical solutions
Stress concentrations

ABSTRACT

This paper presents a homogenization method for unidirectional periodic composite materials reinforced by circular fibres with functionally graded coating layers. The asymptotic homogenization method is adopted, and the relevant cell problem is addressed. Periodicity is enforced by resorting to the theory of Weierstrass elliptic functions. The equilibrium equation in the coating domain is solved in closed form by applying the theory of hypergeometric functions, for different choices of grading profiles. The effectiveness of the present analytical procedure is proved by convergence analysis and comparison with finite element solutions. The influence of microgeometry and grading parameters on the shear stress concentration at the coating/matrix interface is addressed, aimed at the composite optimization in regards to fatigue and debonding phenomena.

1. Introduction

Fibre reinforced composite materials are widely used in engineering practice for their outstanding properties of design versatility and economic convenience (Jones, 1999). It is well known that one of the major issues connected to such composites resides in debonding due to stress concentration at inclusion/matrix interface (Bertrand et al., 1995; Andrianov et al., 2007, 2008). A general way to ameliorate the durability of the material with respect to such a risk is to interpose a coating material between reinforcement and matrix to ensure physical continuity between the two components. This technology is defined as fibre sputtering (Nose et al., 2011; Zhang et al., 2011) and has the general target of strengthening the composite material. It also makes possible to transfer stresses more gradually from one phase to the other, to allow deviation cracks, to make wettability between inclusion and matrix easier, and to avoid chemical reactions (Bertrand et al., 1995; Brendel et al., 2005, 2009; Du et al., 2010).

This work deals with the above introduced problem. In particular, it develops an asymptotic homogenization method to determine the effective longitudinal shear moduli of linear elastic, periodic composites, reinforced by straight circular fibres coated by a layer of cylindrically orthotropic functionally graded material. The present approach permits to develop a quantitative study on how the coating layer grading may reduce the risk of debonding and interface failure. In particular, it is worth noting that grading only a limited part of the inclusion may result in interesting advantages with respect to a different approach (Artioli et al., 2010) where the hypothesis of graduation of the whole inclusion was adopted. In such a way the present results may indicate new design criteria for optimized materials with respect to performance and durability.

The analysis focuses on the antiplane shear deformation state. The method implies the solution of the equilibrium field equation in each of the three subdomains: fibre, coating, and matrix, respectively. Moreover, the solution strategy requires the satisfaction of the equilibrium and displacement continuity laws at the fibre/coating and coating/matrix interfaces, and the satisfaction of the periodicity boundary conditions at the unit-cell boundary as well. Solving the equilibrium field equation is a nontrivial task in the radially-graded coating domain, and a method previously developed by Artioli et al. (2010) is extended to the present case. Several types of grading laws are applied and solved for in closed-form. Such a collection of analytical profiles can be useful as a benchmark for numerical solutions, and to approximate experimental profiles encountered in applications, in the field of antiplane shear deformations, electric or thermal conduction, or electrostatics.

Many procedures for estimating the effective moduli of composites are available in the literature. Some of them are based on the solution for dilute suspensions, whereas others take into account interactions among fibres (see, e.g., Mura, 1987; Milton, 2004; Buryachenko, 2007 and the references cited therein). For periodic microstructures, these interactions are taken into account by imposing periodic boundary conditions at the unit-cell boundary. This issue can be accomplished by using different methods,

* Corresponding author. Tel.: +39 06 7259 7014; fax: +39 06 7259 7005.
E-mail addresses: artioli@ing.uniroma2.it (E. Artioli), bisegna@uniroma2.it (P. Bisegna).

0020-7683/$ - see front matter © 2013 Elsevier Ltd. All rights reserved.
http://dx.doi.org/10.1016/j.ijsolstr.2012.12.014

including Fourier transform (Iwakuma and Nemat-Nasser, 1983; Michel et al., 1999; Bonnet, 2007), elastostatic resonances (Kantor and Bergman, 1982), boundary elements (Helsing, 1995), finite elements (Michel et al., 1999; Wang et al., 2006) or more involved techniques such as the boundary shape perturbation method (Andrianov et al., 2007, 2008), the mean-field homogenization method (Friebel et al., 2006), the average inclusion method (Xun et al., 2004), and the extended electromechanical equivalent inclusion method (Hashemi and Kargarnovin, 2011). In this work, periodicity is enforced following the classical multipole expansion method (Lord Rayleigh, 1892), quite popular in the literature (Perrins et al., 1979; Kalamkarov, 1992; Meguid and Kalamkarov, 1994; Rodríguez-Ramos et al., 2001; Jiang et al., 2004; Chen and Kuo, 2005; Parnell and Abrahams, 2006; Bisegna and Caselli, 2008; Kushch et al., 2008; Artioli et al., 2010). In particular, the cell function over the matrix domain is represented by a linear combination of functions defined in terms of the doubly-periodic Weierstrass ζ function and its derivatives (Whittaker and Watson, 1927; Apostol, 1997), naturally satisfying the periodicity condition at the cell boundary. The actual solution is then computed through the identification of the latter representation, with the Fourier-series representation arising after satisfying the equilibrium field equations in the fibre, coating, and matrix domains, and enforcing the equilibrium and displacement continuity laws at the interfaces. An infinite system of linear algebraic equations is thus obtained, which is truncated to a finite order N and solved.

The paper is organized as follows. In Section 2 the mathematical problem of asymptotic homogenization is introduced and the equilibrium homogenized equation is obtained for the composite material under investigation. Section 3 is the corner stone of the work and is mainly devoted to the cell problem solution based on the use of Fourier series. The relative interface and periodicity boundary condition satisfaction technique is presented as well. The explicit form of the effective constitutive tensor and some considerations on the limit situation of zero-thickness coating close the section. Section 4 reports numerical evidence of the proposed method reliability and of the capability of predicting the influence of grading features and unit cell geometry on the homogenized properties of the composite. Moreover, a comparison with other homogenization approaches available in the literature (Sevostianov et al., 2012) is presented. Finally, the ability to reduce the shear stress concentration at the inclusion/matrix interface by properly designing the coating grading profile is assessed. In Appendix A closed-form solutions are presented for different types of coating grading profiles.

2. Statement of the problem

Reference is made to a composite material constituted of long, parallel fibres with circular cross section, embedded into a surrounding matrix. Fibres are arranged in a regular lattice determined by two families of parallel lines, respectively parallel to the x_1 axis, and forming an angle φ with the latter, as sketched in Fig. 1(a). This geometrical set up can be interpreted as a two dimensional array of unit cells, developing periodically along the x_1 and φ directions. The unit cell, i.e. the microstructure of the composite, can be appreciated in Fig. 1(b). The cell sides measure L_1 and L_2 respectively, and the fibre radius is R. Fibres present a circular coating constituted by a layer of constant thickness δ, made of functionally graded material (Fig. 1(b)).

The effective material shear moduli are obtained here by asymptotic homogenization: to this end, a family of problems is introduced, indexed by a parameter ε scaling the microstructure (Fig. 1(a)). The homogenization limit is obtained by letting ε go to zero.

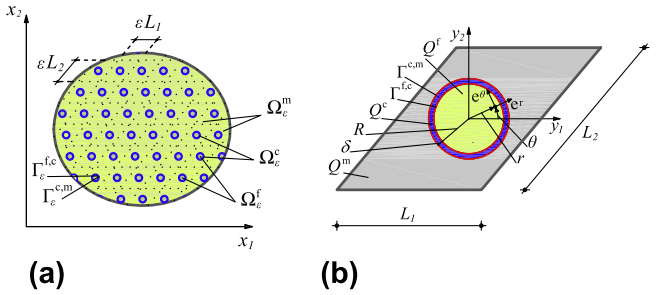

Fig. 1. (a) Geometrical setting of the problem at the macroscale: cross section of the fibrous composite (the fibre size is exaggerated with respect to the sample size, for illustrative purposes). (b) Geometrical setting of the cell (or local) problem at the microscale.

In the framework of antiplane shear deformations, the problem of determining the longitudinal displacement field w_ε in the composite domain is stated as follows:

$$\operatorname{div}(\boldsymbol{G}\nabla w_\varepsilon) = 0, \quad \text{in } \Omega_\varepsilon^f \cup \Omega_\varepsilon^c \cup \Omega_\varepsilon^m; \tag{1}$$

$$[\![\boldsymbol{G}\nabla w_\varepsilon \cdot \boldsymbol{v}]\!] = 0, \quad \text{on } \Gamma_\varepsilon^{f,c} \cup \Gamma_\varepsilon^{c,m}; \tag{2}$$

$$[\![w_\varepsilon]\!] = 0, \quad \text{on } \Gamma_\varepsilon^{f,c} \cup \Gamma_\varepsilon^{c,m}. \tag{3}$$

Here Ω_ε^f, Ω_ε^c and Ω_ε^m denote fibre, coating and matrix domains respectively. Moreover $\Gamma_\varepsilon^{f,c}$ and $\Gamma_\varepsilon^{c,m}$ indicate the ensemble of fibre/coating and coating/matrix interfaces, $\boldsymbol{v}$ is the outward unit vector normal to $\Gamma_\varepsilon^{f,c}$ and $\Gamma_\varepsilon^{c,m}$, respectively. Square brackets $[\![(\cdot)]\!]$ denote the jump of the enclosed quantity across the interface, defined as $[(\cdot)^c - (\cdot)^f]$ on $\Gamma_\varepsilon^{f,c}$ [respectively, $[(\cdot)^m - (\cdot)^c]$ on $\Gamma_\varepsilon^{c,m}$].

Eq. (1) is the field equilibrium equation; (2) accounts for equilibrium at $\Gamma_\varepsilon^{f,c}$ and $\Gamma_\varepsilon^{c,m}$, stipulating the continuity of the normal-to-interface component of the shear stress; (3) prescribes continuity of the displacement field across $\Gamma_\varepsilon^{f,c}$ and $\Gamma_\varepsilon^{c,m}$, respectively. These equations must be complemented by suitable boundary conditions on the boundary of the domain $\Omega = \Omega_\varepsilon^f \cup \Gamma_\varepsilon^{f,c} \cup \Omega_\varepsilon^c \cup \Gamma_\varepsilon^{c,m} \cup \Omega_\varepsilon^m$, though their specification is immaterial for the present treatment.

Fibres, coatings, and matrix are assumed to be linear elastic, and their shear moduli are collected in the constitutive tensor $\boldsymbol{G}$, which specializes in

$$\boldsymbol{G} = \boldsymbol{G}^f \quad \text{in } \Omega_\varepsilon^f, \qquad \boldsymbol{G} = \boldsymbol{G}^c \quad \text{in } \Omega_\varepsilon^c, \qquad \boldsymbol{G} = \boldsymbol{G}^m \quad \text{in } \Omega_\varepsilon^m. \tag{4}$$

Both fibres and matrix are homogeneous and isotropic, so that $\boldsymbol{G}^f = G^f \boldsymbol{I}$ and $\boldsymbol{G}^m = G^m \boldsymbol{I}$, with $\boldsymbol{I}$ the second order identity tensor, being G^f and G^m the fibre and matrix shear modulus, respectively. Fibre coatings are made of a cylindrically-orthotropic material whose moduli are functionally-graded along the radial coordinate (i.e., radially graded). Introducing a polar coordinate system (O, r, θ) as depicted in Fig. 1(b), the coating elasticity tensor is:

$$\boldsymbol{G}^c = (G^r \boldsymbol{e}^r \otimes \boldsymbol{e}^r + G^\theta \boldsymbol{e}^\theta \otimes \boldsymbol{e}^\theta) g(\rho), \tag{5}$$

where

$$\rho = \frac{r}{R} \tag{6}$$

is the radial dimensionless coordinate. The symbols $\boldsymbol{e}^r$ and $\boldsymbol{e}^\theta$ indicate the radial and tangential unit vectors, respectively, $\otimes$ denotes the tensor product, and the dimensionless function $g(\rho)$ expresses the material grading law along the radial direction of the coating. Accordingly, setting $t = \delta/R$, $G^r g(1)$ and $G^\theta g(1)$ [respectively, $G^r g(1+t)$ and $G^\theta g(1+t)$] are the radial and tangential shear moduli at $\Gamma_\varepsilon^{f,c}$ [respectively, $\Gamma_\varepsilon^{c,m}$]. Perfect fibre/coating and coating/matrix interfaces are assumed.

In order to guarantee the well posedness of the above problem, the following hypotheses are made:

$$G^{\mathrm{f}} > 0, \quad G^{\mathrm{r}} > 0, \quad G^{\theta} > 0, \quad G^{\mathrm{m}} > 0, \quad g(\rho) > 0 \quad \text{in } [1, 1+t]. \tag{7}$$

2.1. Homogenized equilibrium equation

The asymptotic homogenization method is employed to derive the homogenized or effective constitutive tensor of the composite material. It is only sketched here for the sake of completeness. The interested Reader may refer, e.g., to Bensoussan et al. (1978) and Sanchez-Palencia (1980).

As shown in Fig. 1(a), two different length scales characterize the problem under consideration. Hence, two different space variables are introduced: the macroscopic one, x, and the microscopic one, $y = x/\varepsilon$, $y \in Q$, being Q the unit cell (see Fig. 1(b)), whose intra-fibre space, fibre-coating interface, coating space, coating-matrix interface and matrix space are denoted by Q^{f}, $\Gamma^{\mathrm{f,c}}$, Q^{c}, $\Gamma^{\mathrm{c,m}}$, and Q^{m}, respectively. Accordingly, the divergence and gradient operators are given by the following relations:

$$\mathrm{div} = \mathrm{div}_x + \frac{1}{\varepsilon}\mathrm{div}_y, \quad \nabla = \nabla_x + \frac{1}{\varepsilon}\nabla_y. \tag{8}$$

An asymptotic expansion of the unknown displacement field is considered in the form:

$$w_\varepsilon(x,y) = w_0(x,y) + \varepsilon w_1(x,y) + \varepsilon^2 w_2(x,y) + \cdots, \tag{9}$$

where w_0, w_1, w_2 are Q-periodic functions in y, and w_1, w_2 have null integral average over Q. Substituting (9) into Problem (1)–(3) and equating the power-like terms of ε, three differential problems for w_0, w_1 and w_2 are obtained, respectively. The problem for w_0 is:

$$\mathrm{div}_y(\boldsymbol{G}\nabla_y w_0) = 0, \quad \text{in } Q^{\mathrm{f}} \cup Q^{\mathrm{c}} \cup Q^{\mathrm{m}}; \tag{10}$$

$$[\![\boldsymbol{G}\nabla_y w_0 \cdot \boldsymbol{v}]\!] = 0, \quad \text{on } \Gamma^{\mathrm{f,c}} \cup \Gamma^{\mathrm{c,m}}; \tag{11}$$

$$[\![w_0]\!] = 0, \quad \text{on } \Gamma^{\mathrm{f,c}} \cup \Gamma^{\mathrm{c,m}}. \tag{12}$$

Problem (10)–(12), taking into account (7), implies that $w_0 = w_0(x)$ (Lene and Leguillon, 1982). The problem for w_1 is:

$$\mathrm{div}_y[\boldsymbol{G}(\nabla_y w_1 + \nabla_x w_0)] = 0, \quad \text{in } Q^{\mathrm{f}} \cup Q^{\mathrm{c}} \cup Q^{\mathrm{m}}; \tag{13}$$

$$[\![\boldsymbol{G}(\nabla_y w_1 + \nabla_x w_0) \cdot \boldsymbol{v}]\!] = 0, \quad \text{on } \Gamma^{\mathrm{f,c}} \cup \Gamma^{\mathrm{c,m}}; \tag{14}$$

$$[\![w_1]\!] = 0, \quad \text{on } \Gamma^{\mathrm{f,c}} \cup \Gamma^{\mathrm{c,m}}. \tag{15}$$

The unknown function w_1 is represented in the form (Bensoussan et al., 1978; Sanchez-Palencia, 1980):

$$w_1(x,y) = -\boldsymbol{\chi}(y) \cdot \nabla_x w_0(x), \tag{16}$$

where the cell function $\boldsymbol{\chi}(y)$ has been introduced. Its components $\chi_h, h = 1,2$, are the unique, null average, Q-periodic solutions of the cell problem:

$$\mathrm{div}_y[\boldsymbol{G}(\nabla_y \chi_h - \boldsymbol{e}_h)] = 0, \quad \text{in } Q^{\mathrm{f}} \cup Q^{\mathrm{c}} \cup Q^{\mathrm{m}}; \tag{17}$$

$$[\![\boldsymbol{G}(\nabla_y \chi_h - \boldsymbol{e}_h) \cdot \boldsymbol{v}]\!] = 0, \quad \text{on } \Gamma^{\mathrm{f,c}} \cup \Gamma^{\mathrm{c,m}}; \tag{18}$$

$$[\![\chi_h]\!] = 0, \quad \text{on } \Gamma^{\mathrm{f,c}} \cup \Gamma^{\mathrm{c,m}}, \tag{19}$$

where $\boldsymbol{e}_h$ is the unit vector parallel to the y_h axis.

Finally, the problem for w_2 is obtained:

$$\mathrm{div}_y[\boldsymbol{G}(\nabla_y w_2 + \nabla_x w_1)] = -\mathrm{div}_x[\boldsymbol{G}(\nabla_y w_1 + \nabla_x w_0)], \quad \text{in } Q^{\mathrm{f}} \cup Q^{\mathrm{c}} \cup Q^{\mathrm{m}}; \tag{20}$$

$$[\![\boldsymbol{G}(\nabla_y w_2 + \nabla_x w_1) \cdot \boldsymbol{v}]\!] = 0, \quad \text{on } \Gamma^{\mathrm{f,c}} \cup \Gamma^{\mathrm{c,m}}; \tag{21}$$

$$[\![w_2]\!] = 0, \quad \text{on } \Gamma^{\mathrm{f,c}} \cup \Gamma^{\mathrm{c,m}}. \tag{22}$$

Integrating (20) in $Q^{\mathrm{f}} \cup Q^{\mathrm{c}} \cup Q^{\mathrm{m}}$, using the Gauss–Green Lemma, adding the three contributions and exploiting (21), the following equation is obtained:

$$\frac{1}{|Q|}\int_{Q^{\mathrm{f}} \cup Q^{\mathrm{c}} \cup Q^{\mathrm{m}}} \mathrm{div}_x[\boldsymbol{G}(\nabla_y w_1 + \nabla_x w_0)]\,\mathrm{d}a = 0, \tag{23}$$

where $\mathrm{d}a$ is the area element of $Q^{\mathrm{f}} \cup Q^{\mathrm{c}} \cup Q^{\mathrm{m}}$ and $|\cdot|$ is the Lebesgue measure. Substituting (16) into (23), the homogenized equation for the macroscopic displacement w_0 is finally derived:

$$\mathrm{div}_x(\boldsymbol{G}^{\#}\nabla_x w_0) = 0. \tag{24}$$

Here $\nabla_x w_0$ is the macroscopic shear strain, and

$$\boldsymbol{G}^{\#} = \frac{1}{|Q|}\int_{Q^{\mathrm{f}} \cup Q^{\mathrm{c}} \cup Q^{\mathrm{m}}} \boldsymbol{G}(\boldsymbol{I} - \nabla_y^{\mathrm{t}}\boldsymbol{\chi})\,\mathrm{d}a \tag{25}$$

is the effective constitutive tensor, where the superscript 't' denotes the transpose. Using the Gauss–Green Lemma, (25) is transformed into:

$$\boldsymbol{G}^{\#} = \boldsymbol{G}^{\mathrm{m}}(1-f) + \frac{\boldsymbol{G}^{\mathrm{f}} f}{(1+t)^2} + \frac{1}{|Q|}\left[\int_{Q^{\mathrm{c}}} \boldsymbol{G}^{\mathrm{c}}\,\mathrm{d}a + \int_{Q^{\mathrm{c}}} (\mathrm{div}_y \boldsymbol{G}^{\mathrm{c}}) \otimes \boldsymbol{\chi}\,\mathrm{d}a + \int_{\Gamma^{\mathrm{f,c}} \cup \Gamma^{\mathrm{c,m}}} [\![\boldsymbol{G}\boldsymbol{v} \otimes \boldsymbol{\chi}]\!]\,\mathrm{d}l\right], \tag{26}$$

where $\mathrm{d}l$ is the line element of $\Gamma^{\mathrm{f,c}}$ and of $\Gamma^{\mathrm{c,m}}$, and $f = \pi(R+\delta)^2/|Q|$ is the total inclusion (fibre plus coating) volume fraction. The preceding equation for $\boldsymbol{G}^{\#}$ can be rewritten in terms of the auxiliary cell function:

$$\tilde{\boldsymbol{\chi}} = \boldsymbol{\chi} - (y_1\boldsymbol{e}_1 + y_2\boldsymbol{e}_2), \tag{27}$$

as follows:

$$\boldsymbol{G}^{\#} = \boldsymbol{G}^{\mathrm{m}} + \frac{1}{|Q|}\int_{Q^{\mathrm{c}}} (\mathrm{div}_y \boldsymbol{G}^{\mathrm{c}}) \otimes \tilde{\boldsymbol{\chi}}\,\mathrm{d}a + \frac{1}{|Q|}\int_{\Gamma^{\mathrm{f,c}} \cup \Gamma^{\mathrm{c,m}}} [\![\boldsymbol{G}\boldsymbol{v} \otimes \tilde{\boldsymbol{\chi}}]\!]\,\mathrm{d}l. \tag{28}$$

Eq. (28) yields the effective shear moduli of the composite material in terms of the solution $\boldsymbol{\chi}$ of the cell problem. The cell function depends on the form assumed for $\boldsymbol{G}^{\mathrm{c}}$ and is derived in closed form for different choices of the coating constitutive law.

In applications, a central role is played by the local shear stress $\boldsymbol{\tau}_\varepsilon = \boldsymbol{G}\nabla w_\varepsilon$ in the composite. The leading-order term of its asymptotic expansion turns out to be:

$$\boldsymbol{\tau}_0 = \boldsymbol{G}(\nabla_x w_0 + \nabla_y w_1) = \boldsymbol{G}(\boldsymbol{I} - \nabla_y^{\mathrm{t}}\boldsymbol{\chi})[\nabla_x w_0]. \tag{29}$$

3. Cell problem

3.1. Fourier series representation

The general solution of the field Eq. (17) is obtained via the following Fourier series representation:

- in the isotropic, homogeneous fibre subdomain Q^{f}

$$\chi_h(r,\theta)|_{Q^{\mathrm{f}}} := \chi_h^{\mathrm{f}}(r,\theta) = y_h + \Re\left[\sum_{k=1}^{+\infty{}^{o}} a_{kh}\rho^k \mathrm{e}^{\mathrm{i}k\theta}\right], \tag{30}$$

- in the cylindrically orthotropic, radially-graded coating subdomain Q^{c}

$$\chi_h(r,\theta)|_{Q^{\mathrm{c}}} := \chi_h^{\mathrm{c}}(r,\theta) = y_h + \Re\left[\sum_{k=-\infty}^{+\infty{}^{o}} b_{kh} W_k(\rho)\mathrm{e}^{\mathrm{i}k\theta}\right], \tag{31}$$

- in the isotropic, homogeneous matrix subdomain Q^{m}

$$\chi_h(r,\theta)|_{Q^{\mathrm{m}}} := \chi_h^{\mathrm{m}}(r,\theta) = y_h + \Re\left[\sum_{k=-\infty}^{+\infty{}^{o}} c_{kh}\rho^k \mathrm{e}^{\mathrm{i}k\theta}\right]. \tag{32}$$

Here $\mathrm{i} = \sqrt{-1}$; the symbol $\Re$ denotes the real part; the sums affected by the apex ^{o} are extended over odd indices only, since the microstructure considered herein (Fig. 1) is centre symmetric with respect to the origin O, so that the solution $\boldsymbol{\chi}$ satisfies the property:

$$\boldsymbol{\chi}(r,\theta) = -\boldsymbol{\chi}(r,\theta+\pi). \tag{33}$$

Moreover, the sum in (30) is extended over positive indices only, in order to enforce the regularity of χ_h at $O \in Q^{\mathrm{f}}$. The functions $W_{\pm k}(\rho)$, $k = 1,\dots,+\infty$, odd k, are any two independent integrals of the equation:

$$W''_{\pm k} + \left(\frac{g'}{g} + \frac{1}{\rho}\right) W'_{\pm k} - \frac{\sigma^2 k^2}{\rho^2} W_{\pm k} = 0, \quad \text{in } (1, 1+t), \tag{34}$$

where $\sigma^2 = G^{\theta}/G^{\mathrm{r}}$ is the anisotropy ratio, and an apex denotes differentiation with respect to ρ. Finally, the quantities a_{kh}, b_{kh}, $b_{(-k)h}$, c_{kh}, $c_{(-k)h}$, $k = 1,\dots,+\infty$, odd k, are complex constants which are determined in the following, by exploiting the interface boundary conditions (18) and (19) on $\Gamma^{\mathrm{f,c}} \cup \Gamma^{\mathrm{c,m}}$ and the periodicity requirement on ∂Q.

3.2. Interface boundary condition

Substituting representations (30)–(32) into the interface boundary conditions (18) and (19), the following equations are obtained, for odd k, and $h = 1, 2$:

$$G^{\mathrm{f}} k a_{kh} = G^{\mathrm{r}} g(1)[b_{kh} W'_k(1) + \bar{b}_{(-k)h} W'_{(-k)}(1)], \tag{35}$$

$$\begin{aligned} &G^{\mathrm{r}} g(1+t)[b_{kh} W'_k(1+t) + \bar{b}_{(-k)h} W'_{(-k)}(1+t)] \\ &\quad = G^{\mathrm{m}} k[c_{kh}(1+t)^{k-1} - \bar{c}_{(-k)h}(1+t)^{-k-1}], \end{aligned} \tag{36}$$

$$a_{kh} = b_{kh} W_k(1) + \bar{b}_{(-k)h} W_{(-k)}(1), \tag{37}$$

$$\begin{aligned} &b_{kh} W_k(1+t) + \bar{b}_{(-k)h} W_{(-k)}(1+t) \\ &\quad = c_{kh}(1+t)^k + \bar{c}_{(-k)h}(1+t)^{-k}, \end{aligned} \tag{38}$$

where an overbar denotes the complex conjugate. Eqs. (35)–(38) allow to express the unknown coefficients a_{kh}, b_{kh}, $b_{(-k)h}$ and c_{kh} as functions of $c_{(-k)h}$ as follows:

$$a_{kh} = \gamma^a_k \bar{c}_{(-k)h}, \quad b_{kh} = \gamma^b_k \bar{c}_{(-k)h}, \quad \bar{b}_{(-k)h} = \gamma^{\bar{b}}_k \bar{c}_{(-k)h}, \quad c_{kh} = \gamma^c_k \bar{c}_{(-k)h}, \tag{39}$$

where

$$\gamma^a_k = -2kG^{\mathrm{m}} G^{\mathrm{r}} g(1)[W'_k(1) W_{(-k)}(1) - W'_{(-k)}(1) W_k(1)]/\psi_{k_{\mathrm{sum}}}, \tag{40}$$

$$\gamma^b_k = -2kG^{\mathrm{m}}[kG^{\mathrm{f}} W_{(-k)}(1) - G^{\mathrm{r}} g(1) W'_{(-k)}(1)]/\psi_{k_{\mathrm{sum}}}, \tag{41}$$

$$\gamma^{\bar{b}}_k = 2kG^{\mathrm{m}}[kG^{\mathrm{f}} W_k(1) - G^{\mathrm{r}} g(1) W'_k(1)]/\psi_{k_{\mathrm{sum}}}, \tag{42}$$

$$\gamma^c_k = (1+t)^{-2k}(\psi_{k_\triangle} + \psi_{k_\circ} - \psi_{k_\star} - \psi_{k_\square})/\psi_{k_{\mathrm{sum}}}, \tag{43}$$

being

$$\begin{aligned} \psi_{k_\star} = (1+t)^{(k+1)} (G^{\mathrm{r}})^2 g(1) g(1+t)[&W'_k(1) W'_{(-k)}(1+t) \\ &- W'_{(-k)}(1) W'_k(1+t)], \end{aligned} \tag{44}$$

$$\begin{aligned} \psi_{k_\triangle} = -k^2 (1+t)^k G^{\mathrm{f}} G^{\mathrm{m}}[&W_k(1+t) W_{(-k)}(1) - W_{(-k)}(1 \\ &+ t) W_k(1)], \end{aligned} \tag{45}$$

$$\begin{aligned} \psi_{k_\square} = k(1+t)^{k+1} G^{\mathrm{f}} G^{\mathrm{r}} g(1+t)[&W'_k(1+t) W_{(-k)}(1) - W'_{(-k)}(1 \\ &+ t) W_k(1)], \end{aligned} \tag{46}$$

$$\begin{aligned} \psi_{k_\circ} = -k(1+t)^k G^{\mathrm{m}} G^{\mathrm{r}} g(1)[&W'_k(1) W_{(-k)}(1+t) \\ &- W'_{(-k)}(1) W_k(1+t)], \end{aligned} \tag{47}$$

$$\psi_{k_{\mathrm{sum}}} = \psi_{k_\star} + \psi_{k_\triangle} + \psi_{k_\square} + \psi_{k_\circ}. \tag{48}$$

3.3. Periodicity condition

The cell function $\boldsymbol{\chi}$ is Q-periodic, i.e., it satisfies:

$$\begin{aligned} \boldsymbol{\chi}^{\mathrm{m}}(y_1 + L_1, y_2) &= \boldsymbol{\chi}^{\mathrm{m}}(y_1, y_2) \\ &= \boldsymbol{\chi}^{\mathrm{m}}(y_1 + L_2 \cos\varphi, y_2 + L_2 \sin\varphi). \end{aligned} \tag{49}$$

This periodicity requirement is enforced by identifying the representation (32) valid in the matrix domain with a linear combination of doubly-periodic basis functions defined in terms of the complex variable

$$z = \frac{y_1 + \mathrm{i} y_2}{L_1} = \frac{r\mathrm{e}^{\mathrm{i}\theta}}{L_1} = \widehat{R}\rho\mathrm{e}^{\mathrm{i}\theta}, \tag{50}$$

where $\widehat{R} = R/L_1$ is the dimensionless fibre radius. Accordingly, the relevant semi-periods are:

$$\omega_1 = \frac{1}{2}, \quad \omega_2 = \frac{\kappa}{2}\mathrm{e}^{\mathrm{i}\varphi}, \tag{51}$$

where $\kappa = L_2/L_1$ is the side ratio of the unit cell. More specifically, the following equation is implemented:

$$\chi^{\mathrm{m}}_h = \sum_{s=1}^{+\infty\,\circ} \sum_{l=1}^{2} w_{slh}\, \Re[B_{sl}(z)], \tag{52}$$

where the coefficients w_{slh} are real unknowns. The functions $B_{sl}(z)$ are chosen following an approach tracing back to the classical Rayleigh multipole expansion method (Lord Rayleigh, 1892; Perrins et al., 1979) and relying on the theory of elliptic functions (Whittaker and Watson, 1927). More specifically, the following choice is made (Kalamkarov, 1992; Meguid and Kalamkarov, 1994; Rodríguez-Ramos et al., 2001; Bisegna and Caselli, 2008; Artioli et al., 2010):

$$B_{sl}(z) = \begin{cases} -\eta_l z + \omega_l \zeta(z), & \text{if } s = 1, \ l = 1,2; \\ \omega_l \frac{\zeta^{(s-1)}(z)}{(s-1)!}, & \text{for } s > 1, \text{ odd } s, \ l = 1,2, \end{cases} \tag{53}$$

where $\zeta(z)$ denotes the Weierstrass Zeta function of semiperiods ω_1, ω_2. It is odd and quasi-periodic, that is:

$$\zeta(z + 2\omega_k) = \zeta(z) + 2\eta_k, \tag{54}$$

with $k = 1,2$ and $\eta_k = \zeta(\omega_k)$. The latter quantities are linked to the semiperiods ω_1, ω_2 by Legendre's relationship:

$$\eta_1 \omega_2 - \eta_2 \omega_1 = \frac{1}{2}\pi\mathrm{i}. \tag{55}$$

Using (54) and (55), and recalling that the derivatives of $\zeta(z)$ are elliptic functions, it is easy to verify that the basis functions $\Re[B_{sl}(z)]$ are indeed doubly periodic, with semiperiods ω_1, ω_2. Only odd functions $B_{sl}(z)$ are introduced here, due to condition (33).

In the cited literature, the unit cell is symmetric with respect to the y_1 and y_2 axes. This implies evenness or oddness properties for the cell function χ^{m}_h, which is consequently represented by the subset of the functions (53) corresponding to $l = 1$ or $l = 2$ only. In this work no such symmetry is assumed, and hence the whole set (53) is considered.

The identification of (32) and (52) is easily obtained by considering the Laurent series of each function $B_{sl}(z)$, having a pole of order s at $z = 0$, as follows:

$$B_{sl}(z) = \sum_{k=1}^{s\,\circ} \frac{v_{ksl}}{z^k} + \sum_{k=1}^{+\infty\,\circ} \xi_{ksl} z^k, \tag{56}$$

where v_{ksl} and ξ_{ksl} are the series coefficients of the singular and regular part of $B_{sl}(z)$, respectively. Those coefficients turn out to be (Artioli et al., 2010):

$$v_{ksl} = \omega_l \delta_{ks}, \quad \xi_{ksl} = -\omega_l \mu_{ks} - \eta_l \delta_{k1} \delta_{s1}. \tag{57}$$

where δ_{ks} is the Krönecker symbol, and, for odd natural numbers k, s,

$$\mu_{ks} = \frac{1}{k+s-1}\binom{k+s-1}{s-1} d_{\frac{k+s}{2}}. \tag{58}$$

Here round brackets denote the binomial coefficient, it has been stipulated that $d_1 = 0$ for ease of notation, and the coefficients d_k, $k \geqslant 2$, are defined by the Laurent series expansion of $\zeta(z)$:

$$\zeta(z) = \frac{1}{z} - \sum_{k=2}^{+\infty} d_k \frac{z^{2k-1}}{2k-1}. \tag{59}$$

They can be easily computed using the following rapidly convergent Fourier series (Apostol, 1997):

$$\frac{d_k}{2k-1} = 2(2\omega_1)^{-2k}\left[\zeta_R(2k) + \frac{(2\pi \mathrm{i})^{2k}}{(2k-1)!}\sum_{n=1}^{+\infty}\sigma_{2k-1}(n)\mathrm{e}^{2\pi \mathrm{i} n\omega_2/\omega_1}\right], \tag{60}$$

where $\zeta_R(\alpha) = \sum_{n=1}^{+\infty} n^{-\alpha}$ is the Riemann Zeta function, and $\sigma_\alpha(n) = \sum_{l|n} l^\alpha$ is the divisor function.

Using (56) and (57), (52) is transformed into:

$$\chi_h^{\mathrm{m}} = \Re\left[\sum_{k=1}^{+\infty o}\left(\sum_{l=1}^{2}\omega_l w_{klh}\right)z^{-k} - \sum_{k=1}^{+\infty o}\left(\sum_{s=1}^{+\infty o}\sum_{l=1}^{2}\omega_l\mu_{ks}w_{slh}\right)z^k - \sum_{l=1}^{2}\eta_l w_{1lh} z\right], \tag{61}$$

which, recalling (50), is compared term-by-term to (32) and yields, for odd natural numbers k:

$$\widehat{R}^k c_{(-k)h} = \sum_{l=1}^{2}\omega_l w_{klh}, \tag{62}$$

$$\widehat{R}^{-k}c_{kh} + L_1 g_h\delta_{k1} = -\sum_{s=1}^{+\infty o}\sum_{l=1}^{2}\omega_l\mu_{ks}w_{slh} - \sum_{l=1}^{2}\eta_l\delta_{k1}w_{1lh}, \tag{63}$$

where

$$g_h = \begin{cases} 1, & \text{if } h = 1, \\ -\mathrm{i}, & \text{if } h = 2, \end{cases} \tag{64}$$

so that $y_h = \Re(g_h \mathrm{r}\mathrm{e}^{\mathrm{i}\theta})$.

3.4. Solution of the cell problem and effective constitutive tensor

The solution of the cell problem is achieved by substituting (62) and (63) into the interface boundary condition $(39)_4$, leading to:

$$-\widehat{R}^k\sum_{s=1}^{+\infty o}\sum_{l=1}^{2}\omega_l\mu_{ks}w_{slh} - \widehat{R}\sum_{l=1}^{2}\eta_l\delta_{k1}w_{1lh} - Rg_h\delta_{k1} = \gamma_k^{\mathrm{c}}\widehat{R}^{-k}\sum_{l=1}^{2}\overline{\omega_l}w_{klh}. \tag{65}$$

Making the position (Nicorovici et al., 1993)

$$q_{slh} = \frac{\sqrt{s}}{\widehat{R}^s}w_{slh}, \tag{66}$$

the following infinite set of linear algebraic equations is obtained, for odd natural numbers k:

$$\gamma_k^{\mathrm{c}}\sum_{l=1}^{2}\overline{\omega_l}q_{klh} + \sum_{s=1}^{+\infty o}S_{ks}\sum_{l=1}^{2}\omega_l q_{slh} + \delta_{k1}\widehat{R}^2\sum_{l=1}^{2}\eta_l q_{1lh} = -Rg_h\delta_{k1}, \tag{67}$$

where $S_{ks} = \mu_{ks}\widehat{R}^{k+s}\sqrt{k/s}$ turns out to be a symmetric matrix (Nicorovici et al., 1993). Taking the real and imaginary parts of the latter allows to compute the real unknowns q_{slh}, which in turn determine w_{slh} via (66), $c_{(-k)h}$ via (62), c_{kh}, $b_{(-k)h}$, b_{kh} and a_{kh} via (39). Hence, the cell functions χ_h^{m}, χ_h^{f} are computed by (30)–(32).

Of course, it is necessary to truncate the system (67) to a finite order N, amounting to taking into account a finite number of coefficients in the representations (30)–(32). It is shown in Section 4 that taking N of the order of units yields accurate results for composite microgeometry configurations of interest.

Finally, the effective material tensor $\boldsymbol{G}^{\#}$ follows from (28). After some algebra, it turns out that:

$$G_{hj}^{\#} = G^{\mathrm{m}}\delta_{hj} + \frac{f}{R(1+t)^2}\Re[G^{\mathrm{m}}(\overline{g}_h c_{1j}(1+t)^2 + g_h c_{(-1)j}) - G^{\mathrm{r}}(\Psi^{(+)}\overline{g}_h b_{1j} + \Psi^{(-)}c_h b_{(-1)j}) - G^{\mathrm{f}}\overline{g}_h a_{1j}], \tag{68}$$

with

$$\Psi^{(\pm)} = \int_1^{1+t} g(\rho)[\rho W'_{(\pm1)}(\rho) + \sigma^2 W_{(\pm1)}(\rho)]\,\mathrm{d}\rho.$$

For a given grading profile, the above coefficients $\Psi^{(\pm)}$, as well as the coefficients $W_{(\pm k)}(1)$, $W_{(\pm k)}(1+t)$, $W'_{(\pm k)}(1)$, and $W'_{(\pm k)}(1+t)$ entering (40)–(47), can be computed via numerical integration of (34). However, closed-form solutions to the latter problem for several families of grading profiles are presented in Appendix A.

3.5. Vanishing coating-thickness limit configuration

In this section the limit configuration of the coating which progressively becomes a zero-thickness fibre/matrix interface is considered, i.e., the limit as t approaches zero is taken. Two different limits are computed, either without rescaling, or rescaling, the coating stiffness, thus recovering known homogenization solutions, respectively involving composites with perfect, or imperfect zero-thickness, fibre/matrix interfaces. The latter limit establishes a connection between different models describing imperfect interfaces (Sevostianov et al., 2012).

First, G^{r} and G^{θ} are kept as constants. Since in the limiting process the shear stress in the coating remains stable with respect to t, so does the shear strain. Consequently, as the coating thickness approaches 0, the traces on $\Gamma^{\mathrm{f,c}}$ and $\Gamma^{\mathrm{c,m}}$ of the cell functions χ_h become equal, i.e., the perfect-interface condition is attained. In fact, it is found that:

$$\psi_{k_\star} = [G^{\mathrm{r}}g(1)]^2[W'_k(1)W''_{(-k)}(1) - W'_{(-k)}(1)W''_k(1)]t + o(t), \tag{69}$$

$$\psi_{k_\triangle} = -k^2 G^{\mathrm{f}}G^{\mathrm{m}}C\,t + o(t), \tag{70}$$

$$\psi_{k_\square} = kG^{\mathrm{f}}G^{\mathrm{r}}g(1)C + o(1), \tag{71}$$

$$\psi_{k_\circ} = -kG^{\mathrm{m}}G^{\mathrm{r}}g(1)C + o(1), \tag{72}$$

$$\psi_{k_{\mathrm{sum}}} = k(G^{\mathrm{f}} - G^{\mathrm{m}})G^{\mathrm{r}}g(1)C + o(1), \tag{73}$$

where $C = W'_k(1)W_{(-k)}(1) - W'_{(-k)}(1)W_k(1)$. Accordingly, coefficients (40)–(43) are given by:

$$\gamma_k^a = -\frac{2G^{\mathrm{m}}}{G^{\mathrm{f}} - G^{\mathrm{m}}} + o(1), \tag{74}$$

$$\gamma_k^b = -\frac{2G^{\mathrm{m}}[kG^{\mathrm{f}}W_{(-k)}(1) - G^{\mathrm{r}}g(1)W'_{(-k)}(1)]}{(G^{\mathrm{f}} - G^{\mathrm{m}})G^{\mathrm{r}}g(1)C} + o(1), \tag{75}$$

$$\gamma_k^{\bar{b}} = \frac{2G^{\mathrm{m}}[kG^{\mathrm{f}}W_k(1) - G^{\mathrm{r}}g(1)W'_k(1)]}{(G^{\mathrm{f}} - G^{\mathrm{m}})G^{\mathrm{r}}g(1)C} + o(1), \tag{76}$$

$$\gamma_k^c = -\frac{G^{\mathrm{f}} + G^{\mathrm{m}}}{G^{\mathrm{f}} - G^{\mathrm{m}}} + o(1). \tag{77}$$

As expected, recalling (39), it follows that the left-hand side of (37) approaches the right-hand side of (38), i.e., the perfect-interface

condition is obtained. Moreover, as $t \to 0$, γ_k^a and γ_k^c coincide with the corresponding coefficients of Artioli et al. (2010) (refer Eqs. (39) and (40) therein, specialized to the case of homogeneous isotropic fibre with shear modulus G^f and perfect interface, i.e. $RD \to \infty$). Also the effective constitutive tensors consistently coincide and are found to be:

$$G^{\#}_{hj} = G^m \delta_{hj} + \frac{f}{R}\Re[G^m(\overline{g}_h c_{1j} + g_h c_{(-1)j}) - G^f \overline{g}_h a_{1j}]. \tag{78}$$

The further limit case of a rigid fibre inclusion with perfect fibre/matrix interface is then obtained by taking the limit of (74) and (77) as $G^f \to +\infty$. It turns out that $\gamma_k^a \to 0$, $G^f\gamma_k^a \to -2G^m$, $\gamma_k^c \to -1$, and, using (39), the homogenized material moduli reduce to:

$$G^{\#}_{hj} = G^m\left[\delta_{hj} + \frac{f}{R}(\overline{g}_h \bar{c}_{(-1)j} + g_h c_{(-1)j})\right]. \tag{79}$$

Likewise, this result is found in the corresponding limit configuration of the model presented by Artioli et al. (2010).

A different limiting process is obtained by concentrating the coating compliance as $t \to 0$. To this end, use is made of the following scaling of the coating material moduli in terms of t (Lene and Leguillon, 1982):

$$G^r = G_0^r \frac{t}{t_0}, \quad G^\theta = G_0^\theta \frac{t}{t_0}, \tag{80}$$

being G_0^r, G_0^θ and t_0 reference material parameters and dimensionless coating thickness, respectively. With this scaling, the shear stress in the coating remains stable with respect to t and the shear strain diverges as t_0/t due to the stiffness scaling. Consequently the jump of the traces on $\Gamma^{f,c}$ and $\Gamma^{c,m}$ of the cell functions χ_h remains stable and proportional to the shear stress, and a zero-thickness linear spring interface model (Lene and Leguillon, 1982; Hashin, 1991; Bigoni et al., 1998; Artioli et al., 2010) is obtained in the limit.

Substituting (80) into (44)–(47) gives:

$$\psi_{k_\star} = \left[\frac{G_0^r g(1)}{t_0}\right]^2 [W_k'(1)W''_{(-k)}(1) - W'_{(-k)}(1)W_k''(1)]t^3 + o(t^3), \tag{81}$$

$$\psi_{k_\triangle} = -k^2 G^f G^m C t + o(t), \tag{82}$$

$$\psi_{k_\square} = \frac{k G^f G_0^r g(1)}{t_0} C t + o(t), \tag{83}$$

$$\psi_{k_\circ} = -\frac{k G^m G_0^r g(1)}{t_0} C t + o(t), \tag{84}$$

$$\psi_{k_{\text{sum}}} = k(G^f - G^m)\frac{G_0^r g(1)}{t_0} C t - k^2 G^f G^m C t + o(t). \tag{85}$$

Accordingly, coefficients (40)–(43) become:

$$\gamma_k^a = \frac{2\frac{G_0^r g(1)}{t_0 G^f}}{k + \frac{G_0^r g(1)}{t_0}\left(\frac{1}{G^f} - \frac{1}{G^m}\right)} + o(1), \tag{86}$$

$$\gamma_k^b = \frac{2k}{k + \frac{G_0^r g(1)}{t_0}\left(\frac{1}{G^f} - \frac{1}{G^m}\right)} \frac{W_{(-k)}(1)}{Ct} + o\left(\frac{1}{t}\right), \tag{87}$$

$$\gamma_k^{\bar{b}} = \frac{-2k}{k + \frac{G_0^r g(1)}{t_0}\left(\frac{1}{G^f} - \frac{1}{G^m}\right)} \frac{W_k(1)}{Ct} + o\left(\frac{1}{t}\right), \tag{88}$$

$$\gamma_k^c = \frac{k + \frac{G_0^r g(1)}{t_0}\left(\frac{1}{G^f} + \frac{1}{G^m}\right)}{k + \frac{G_0^r g(1)}{t_0}\left(\frac{1}{G^f} - \frac{1}{G^m}\right)} + o(1). \tag{89}$$

Using (39) and noting that $\Psi^{(\pm)}/t$ stay bounded as $t \to 0$, it follows that (78) holds also in this case. Hence, the effective moduli computed in Artioli et al. (2010) are recovered (refer Eqs. (39) and (59) therein, specialized to the case of homogeneous isotropic fibre with shear modulus G^f), provided that the following identification is enforced:

$$D = \frac{G_0^r g(1)}{t_0 R}, \tag{90}$$

relating the imperfect-interface stiffness D introduced in Artioli et al. (2010) (refer Eqs. (3) and (19) therein) to the coating properties $G_0 g(1)$ and $t_0 R$.

4. Numerical results and discussion

This section is dedicated to validating the present analytical procedure and to discussing the influence of geometrical and material parameters on the overall material behaviour.

The analysis is developed using the dimensionless parameters φ, $\kappa = L_2/L_1$, $t = \delta/R$, $f = \pi R^2(1+t)^2/|Q|$, $\sigma^2 = G^\theta/G^r$ previously introduced, and the following ones:

- fibre/matrix stiffness ratio $\xi = G^f/G^m$;
- fibre/coating stiffness ratio $\mu = G^f/(G^r g(1))$;
- grading intensity factor $\omega = g(1)/g(1+t)$;

An isotropic coating material is assumed, thus $\sigma = 1$. Moreover, grading profiles fitting the fibre and matrix material properties (Fig. 2), i.e. $G^r g(1) = G^f$, $G^r g(1+t) = G^m$, are considered. Hence, $\omega = \xi$ and $\mu = 1$. Finally, the simulations refer to exponentially-graded coatings: in particular, $g(\rho)$ follows (A.2) below. In order to fulfil the condition $\omega = \xi$, the involved grading parameters satisfy the following relations (one is the inverse of the other):

$$\lambda = [(1+t)^q - 1]^{-1}\log\xi, \quad q = \frac{\log(1 + \lambda^{-1}\log\xi)}{\log(1+t)}. \tag{91}$$

4.1. Convergence, accuracy and validation

As it was anticipated in Section 3.4, the infinite system (67) needs to be truncated to a finite order N. Here it is ascertained how fast convergence is achieved with respect to N, and which value of N is required to give the effective shear moduli to some chosen relative accuracy.

Reference is made to a regular hexagonal arrangement, for different values of the volume fraction and a fixed dimensionless coating thickness t. Fig. 3(a) shows that the proposed analytical

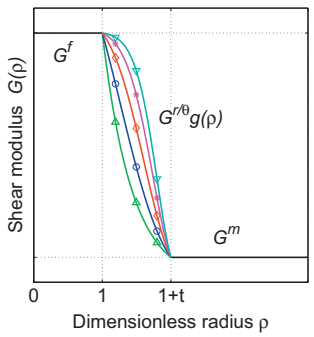

Fig. 2. Shear moduli versus radial dimensionless coordinate ρ. Exponential grading profile (refer (A.2) and (91)), $\omega = \xi$, $\mu = 1$, $\sigma = 1$. $q = 1$ – green upper triangles; $q = 3$ – blue circles; $q = 5$ – red diamonds; $q = 7$ – magenta stars; $q = 9$ – cyan lower triangles. (For interpretation of the references to colour in this figure legend, the reader is referred to the web version of this article.)

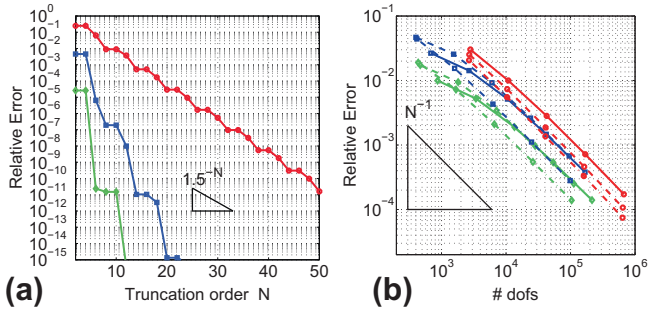

Fig. 3. (a) Convergence property of the present approach: relative error on effective modulus $G^{\#}$ versus truncation order N. Overkill solution: present approach, $N = 100$. (b) Convergence of FEM solution to present solution ($N = 100$): relative error on effective modulus $G^{\#}$ versus number of FEM degrees of freedom. Cell geometry: $\kappa = 1$, $\varphi = \pi/3$ (regular hexagonal arrangement), $t = 1/8$ (a), $t = 1/4$ – dash-dot line (b), $t = 1/8$ – dot line (b), $t = 1/16$ – solid line (b); $f = 0.3$ – green diamonds, $f = 0.6$ – blue squares, $f = 0.9$ – red circles. Exponential grading profile (refer (A.2) and (91)), $\lambda = \log 4$, $\omega = \xi = 50$, $\mu = 1$, $\sigma = 1$. (For interpretation of the references to colour in this figure legend, the reader is referred to the web version of this article.)

scheme exhibits an exponential asymptotic rate of convergence, which turns out to be higher for lower volume fraction values.

Table 1 shows the minimum value of N required for the effective shear modulus $G^{\#}$ to have a relative accuracy of 10^{-2}, 10^{-4} or 10^{-6}, respectively. This value increases with volume fraction f and with fibre/matrix contrast factor ξ (Perrins et al., 1979).

Validation of the present analytical approach is obtained by comparison with a standard finite-element solution. Numerical results are obtained using the Comsol Multiphysics® software (COMSOL AB, 2008), which easily allows to prescribe periodic boundary conditions on the unit-cell boundary.

Fig. 3(b) reports on an hexagonal unit cell with three different values of the volume fraction and the same material parameters as in Fig. 3(a). h-convergence of the finite element solution is assessed, for a linear Lagrange triangular finite element discretization of the unit cell domain. The relative error on the homogenized shear modulus $G^{\#}$ is computed with respect to a reference solution obtained using the proposed analytical method ($N = 100$) and plotted versus the total number of degrees of freedom, in a log–log plot. The correct asymptotic convergence properties exhibited by the adopted linear elements shows that the FEM solution converges to the present analytical one, confirming the method robustness and reliability.

4.1.1. Rigid inclusion with zero-thickness coating

The special case of rigid inclusions with zero-thickness perfect fibre/matrix interface is usually checked as it involves computational difficulties. A comparison is presented between the asymptotic method in Andrianov et al. (2007), the multipole expansion method in Perrins et al. (1979) and the present analytical solution. Results for the effective shear modulus of a composite with a square array of rigid cylinders are presented in Table 2 which indicates an optimal agreement with Perrins approach and a very good agreement with Andrianov method even for fibre volume fractions close to the packaging limit of the unit cell.

Table 1
Present analytical solution. Regular hexagonal cell with $t = 1/16$. Exponential grading profile (refer (A.2) and (91)), $\lambda = \log(600/\xi)$, $\omega = \xi$, $\mu = 1$, $\sigma = 1$. Minimum order N required to give the effective shear modulus to the relative accuracy A of 10^{-2}, 10^{-4} and 10^{-6}. N is listed for various values of the volume fraction f and of the fibre/matrix contrast factor ξ.

f	$A = 10^{-2}$			$A = 10^{-4}$			$A = 10^{-6}$		
	ξ			ξ			ξ		
	5	50	500	5	50	500	5	50	500
0.1	1	1	1	1	1	1	1	1	1
0.2	1	1	1	1	1	1	3	3	3
0.3	1	1	1	1	1	1	3	3	3
0.4	1	1	1	3	3	3	3	3	3
0.5	1	1	1	3	3	3	3	3	3
0.6	1	1	1	3	3	3	4	4	4
0.7	3	3	3	4	4	4	6	7	7
0.8	3	3	3	4	6	7	7	9	9
0.9	4	7	10	9	13	19	12	19	28

Table 2
Rigid inclusion with zero-thickness coating. Square cell: rigid fibres with zero-thickness coatings. Nondimensional effective shear modulus $G^{\#}/G^{m}$ for various values of the fibre volume fraction. Method: P, 1979 – (Perrins et al., 1979); A, 2007 – (Andrianov et al., 2007); and present analysis – Eq. (79).

Vol. fract. f	P, 1979	A, 2007	Present solution
0.1	1.222	1.223	1.222
0.2	1.500	1.506	1.500
0.3	1.860	1.879	1.860
0.4	2.351	2.395	2.351
0.5	3.080	3.172	3.080
0.6	4.342	4.517	4.342
0.7	7.433	7.769	7.433
0.74	11.01	11.46	11.01
0.76	15.44	15.99	15.44
0.77	20.43	21.04	20.43
0.78	35.93	36.60	35.94
0.783	–	55.58	54.94
0.784	–	73.08	72.58
0.785		136.8	137.9

4.2. Comparison with other homogenization approaches

A comparison is here provided with the methods proposed in the work by Sevostianov et al. (2012) which focuses on the modelling of heterogeneous materials with imperfect bonding between the matrix and the inclusion, in the shape of parallel circular cylinders, and on the estimation of the influence of interphase layers on the effective elastic properties of fibre reinforced composites. The comparison is carried out with the so called *Differential approach model*, which evaluates the elastic constants of an equivalent homogeneous inclusion that has the radius of the core plus the interphase thickness and produces the same effect on the overall property. Moreover, the *Three-phase model* is considered, leading to the expression of the properties of an equivalent homogeneous medium through the solution of suitable local problems. The comparison comprehends also the *Spring model*, taking into account the imperfect interface by means of a layer of mechanical springs of zero thickness.

The case of a composite with a square array of inclusions having homogeneous coating with $f = 0.5$, $t = 10^{-3}$, $\xi = 10$, and different coating-to-matrix stiffness ratio is taken into consideration. Results obtained with the above cited methods and the present approach are reported in Fig. 4. An excellent agreement can be observed with the Three-phase formulation which results quite similar to the proposed methodology in the case of a homogeneous coating material.

4.3. Parametric analysis

The influence of the microgeometry parameters κ and φ is addressed in Fig. 5(a) and (b). In particular, rectangular geometries ($\varphi = \pi/2$) with various unit-cell aspect ratios κ are considered in Fig. 5(a), whereas rhombic geometries ($\kappa = 1$) with various values of the unit-cell skewness φ are considered in Fig. 5(b). The coating material is isotropic and exponentially graded. The dimensionless principal effective upper ($G_1^{\#}$) and lower ($G_2^{\#}$) moduli are plotted versus the inclusion volume fraction f. All curves are monotonically

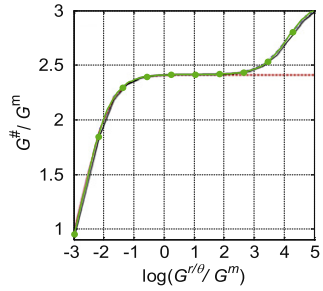

Fig. 4. Comparison between present results and Sevostianov et al. (2012). Normalized effective modulus $G^{\#}/G^{m}$ versus logarithmic coating-to-matrix stiffness ratio. Square arrays with homogeneous coatings: $f = 0.5$, $t = 10^{-3}$, $\xi = 10$. Differential approach model – black solid line; Three-phase model – blue dash-dotted line; Spring model – red dotted line; Present approach – green continuous line with bullets. (For interpretation of the references to colour in this figure legend, the reader is referred to the web version of this article.)

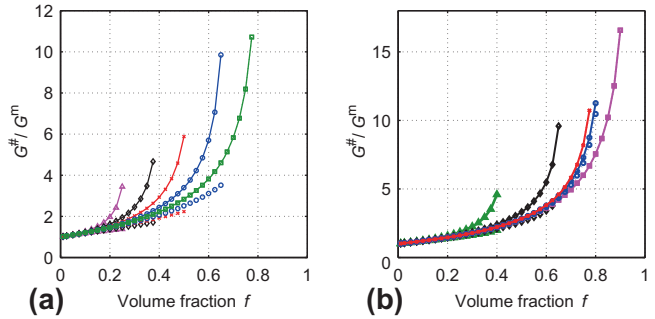

Fig. 5. Principal effective upper modulus $G_1^{\#}$ (continuous line) and lower modulus $G_2^{\#}$ (dotted line) versus fibre volume fraction f, $t = 1/8$. Exponential grading profile (refer (A.2) and (91)), $\lambda = \log 4$, $\omega = \xi$, $\mu = 1$, $\sigma = 1$. (a) Rectangular geometry: $\varphi = \pi/2$; $\kappa = 1$ – magenta squares, $\kappa = 1.2$ – blue circles, $\kappa = 1.5$ – red crosses, $\kappa = 2$ – black diamonds, $\kappa = 3$ – green triangles. (b) Rhombic geometry: $\kappa = 1$; $\varphi = \pi/6$ – green triangles, $\varphi = \pi/4$ – black diamonds, $\varphi = \pi/3$ – magenta squares, $\varphi = 5\pi/12$ – blue circles, $\varphi = \pi/2$ – red crosses. (For interpretation of the references to colour in this figure legend, the reader is referred to the web version of this article.)

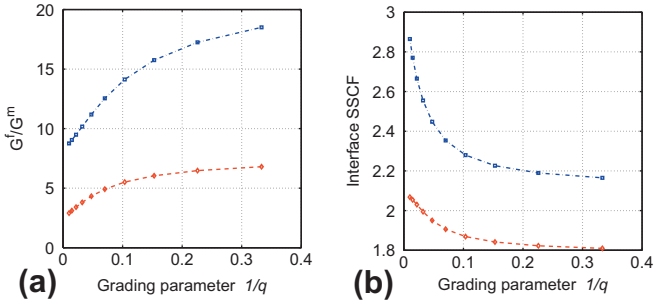

Fig. 6. Composite material with a granted effective modulus $G^{\#}/G^{m}$. (a) Required fibre/matrix stiffness ratio $G^{f}/G^{m} = \xi$, and (b) coating/matrix interface shear stress concentration factor, versus grading parameter $1/q$. Exponential grading profile (refer (A.2) and (91)), $\omega = \xi$, $\mu = 1$, $\sigma = 1$. Square geometry, $f = 0.78$, $t = 2$. $G^{\#}/G^{m} = 2$ – red diamonds; $G^{\#}/G^{m} = 5$ – blue squares. (For interpretation of the references to colour in this figure legend, the reader is referred to the web version of this article.)

increasing, because fibres and coatings are stiffer than the matrix. Each curve terminates at the volume fraction corresponding to the relevant packaging limit; near that limit, the upper modulus is highly sensitive to the volume fraction.

4.4. The shear stress concentration factor

In this section, the analysis points at assessing the reduction of shear stress concentration in the composite, by properly choosing the grading profile $g(\rho)$, keeping fixed the effective shear stiffness of the composite material.

Reference is made to a square cell geometry of volume fraction $f = 0.78$, i.e., near to the packaging limit. The effective stiffness tensor $\boldsymbol{G}^{\#}$ of the composite is isotropic. An exponential grading profile for the coating is considered. The fibre/matrix stiffness ratio $G^{f}/G^{m} = \xi$ required in order to achieve a prescribed dimensionless effective shear stiffness $G^{\#}/G^{m}$ is reported in Fig. 6(a) versus the grading parameter $1/q$. In this way, classes of graded composites with the same effective stiffness are obtained and compared.

An indicator of the performance of the material in terms of shear stresses at the coating/matrix interface is constructed introducing the interface shear stress concentration factor (SSCF), defined as the highest ratio between the L^{∞} norm of the normal component of the shear stress at the $\rho = 1 + t$ interface in the graded composite, and the same quantity in the homogenized material, under all the macroscopic shear strains $\nabla_x w_0$:

$$\text{Interface SSCF} = \sup_{\nabla_x w_0} \frac{\sup_{\rho=1+t} |\boldsymbol{\tau}_0 \cdot \boldsymbol{\nu}|}{G^{\#}|\nabla_x w_0|}. \tag{92}$$

The interface SSCF is reported in Figs. 6(b) as a function of $1/q$, for $G^{\#}/G^{m} = 2$, and 5. A reduction of the shear stress of 20% for higher values of the parameter $1/q$ can be appreciated. Hence, properly grading the elastic properties of the coatings leads to a decrease of interfacial stress concentration, for a given overall stiffness of the material. This result raises attention on innovative composite materials, enhanced in terms of strength with respect to debonding phenomena.

5. Conclusion

This work deals with the determination of the effective longitudinal shear moduli of a unidirectional periodic composite material reinforced with circular fibres coated by a layer of cylindrically orthotropic functionally graded material. A closed form expression for the overall constitutive moduli is obtained applying the asymptotic homogenization theory and Fourier series expansion for the solution of equilibrium equations as well as the theory of Weierstrass elliptic functions for the analytical satisfaction of periodicity boundary conditions. This closed-form expression of the effective shear moduli is presented for a representative set of grading functions and for a general unit cell geometry. An asymptotic analysis of the limit configuration of vanishing coating thickness is performed for validation purposes. Accuracy and efficiency are demonstrated by comparison with a finite element solution on a number of benchmark cases. The numerical implementation of the proposed method shows exponential asymptotic convergence rate with respect to the truncation order of the involved series representations. An analysis on the influence that grading and geometric parameters can have on the reduction of shear stress concentration at coating/matrix interface points at a possible way to design optimized materials in regard to durability with respect to fatigue and debonding problems.

Appendix A. Grading profiles

Closed-form solutions of problem (34) are herein briefly resumed for different grading profiles $g(\rho)$; the relative solution approaches being traceable in Artioli et al. (2010) for instance. In the following, for every odd positive integer k, W_k and $W_{(-k)}$ will de-

note any two independent integrals of (34), assuming, conventionally, that W_k is the regular one at $\rho = 0$.

A.1. Homogeneous material

In this case, $g(\rho) = 1$, and Eq. (34) admits the solutions:

$$W_{(\pm k)}(\rho) = \rho^{\pm \sigma k}. \tag{A.1}$$

A.2. Exponential grading function

The grading function

$$g(\rho) = \exp(-\lambda \rho^q), \tag{A.2}$$

with λ and $q > 0$ material parameters leads to:

$$W_k(\rho) = \rho^{\sigma k}\, {}_1F_1(a_k; b_k; \lambda \rho^q), \tag{A.3}$$

$$W_{(-k)}(\rho) = \rho^{\sigma k}\, U(a_k; b_k; \lambda \rho^q), \tag{A.4}$$

where ${}_1F_1(a_k; b_k; \lambda \rho^q)$ and $U(a_k; b_k; \lambda \rho^q)$ are the confluent hypergeometric function of the first kind and second kind, respectively (Abramowitz and Stegun, 1965), and $a_k = \sigma k/q$, $b_k = 1 + 2\sigma k/q$.

A.3. Special grading functions

A general strategy for the solution of (34) with several types of grading functions can be derived reasoning as in Artioli et al. (2010). The results relevant to the present problem are reported below.

A.3.1. Squared-Bessel grading function

The grading function:

$$g = J_v^2(\lambda \rho), \quad [\text{respectively, } g = Y_v^2(\lambda \rho)], \tag{A.5}$$

where J_v [respectively, Y_v] is the first-kind [respectively, second-kind] Bessel function, yields the closed-form solution:

$$W_k = \frac{J_{v_k}(\lambda \rho)}{J_v(\lambda \rho)}, \quad \left[\text{respectively, } W_k = \frac{J_{v_k}(\lambda \rho)}{Y_v(\lambda \rho)}\right], \tag{A.6}$$

$$W_{(-k)} = \frac{Y_{v_k}(\lambda \rho)}{J_v(\lambda \rho)}, \quad \left[\text{respectively, } W_{(-k)} = \frac{Y_{v_k}(\lambda \rho)}{Y_v(\lambda \rho)}\right], \tag{A.7}$$

where $v_k = \sqrt{v^2 + \sigma^2 k^2}$. A grading profile in the form of a squared modified Bessel function of first or second kind, i.e., $I_v^2(\lambda \rho)$ or $K_v^2(\lambda \rho)$ induces an analogous solution as well.

A.3.2. Squared-hypergeometric grading material

The general solution strategy proposed in Artioli et al. (2010), referring to the theory of hypergeometric differential equations, leads to a numerous class of possible grading functions.

Power-law grading function. Choosing:

$$g(\rho) = \rho^{2\alpha}, \tag{A.8}$$

yields the closed-form solution:

$$W_{(\pm k)} = \rho^{\pm \alpha_k - \alpha}, \tag{A.9}$$

with $\alpha_k = \sqrt{\alpha^2 + \sigma^2 k^2}$.

Binomial-power-law grading function. The following profile is considered:

$$g(\rho) = (1 - \lambda \rho)^{\nu}, \tag{A.10}$$

where the parameter λ must be less than $1/(1 + t)$, so that g does not vanish for $\rho \in [1, 1 + t]$. The case $\lambda = 0$ implies homogeneous fibres. If $0 < \lambda < 1/(1 + t)$, the following closed-form solution is obtained:

$$W_{(\pm k)}(\rho) = (\lambda \rho)^{\pm \alpha_k}\, {}_2F_1(\pm \alpha_k + \beta_k + \gamma, \pm \alpha_k - \beta_k + \gamma; 1 \pm 2\alpha_k; \lambda \rho), \tag{A.11}$$

with $\alpha_k = \sigma k$, $\beta_k = \sqrt{\nu^2/4 + \sigma^2 k^2}$. If $\lambda < 0$, it follows that:

$$W_{(\pm k)}(\rho) = (1 - \lambda \rho)^{-\beta_k - \gamma} \left(\frac{-\lambda \rho}{1 - \lambda \rho}\right)^{\pm \alpha_k} \cdot {}_2F_1\left(\pm \alpha_k + \beta_k + \gamma, 1 \pm \alpha_k + \beta_k - \gamma; 1 \pm 2\alpha_k; \frac{-\lambda \rho}{1 - \lambda \rho}\right). \tag{A.12}$$

Polynomial-law grading functions.

- the grading function $g(\rho) = (\lambda \rho)^{-\frac{1}{2}}(1 - \lambda \rho)^{\frac{1}{2}} T_n^2(1 - 2\lambda \rho)$, where T_n denotes the Chebyshev polynomial of order n, yields the closed-form solution:

$$W_{(\pm k)}(\rho) = \frac{(\lambda \rho)^{\pm \alpha_k + \frac{1}{4}}\, {}_2F_1(\pm \alpha_k + \beta_k + \gamma, \pm \alpha_k - \beta_k + \gamma; 1 \pm 2\alpha_k; \lambda \rho)}{T_n(1 - 2\lambda \rho)}; \tag{A.13}$$

- the grading function $g(\rho) = (1 - \lambda \rho) P_n^2(1 - 2\lambda \rho)$, where P_n denotes Legendre's polynomial of order n, yields the closed-form solution:

$$W_{(\pm k)}(\rho) = \frac{(\lambda \rho)^{\pm \sigma k}\, {}_2F_1(\pm \sigma k + \beta_k + \frac{1}{2}, \pm \sigma k - \beta_k + \frac{1}{2}; 1 \pm 2\sigma k; \lambda \rho)}{P_n(1 - 2\lambda \rho)}. \tag{A.14}$$

Analogous results involving Gegenbauer's polynomials $C_n^{(\alpha)}$ and Jacobi's polynomials $P_n^{(\alpha,\beta)}$ can be derived. Throughout these derivations, $\alpha_k = \sqrt{\alpha^2 + \sigma^2 k^2}$, $\beta_k = \sqrt{\beta^2 + \sigma^2 k^2}$ and the parameter λ must be chosen such that $g(\rho) > 0$ in $[1, 1 + t]$.

Other grading profiles.

- the grading function $g(\rho) = (\lambda \rho)^{-1}(1 - \lambda \rho)\log^2(1 - \lambda \rho)$, yields the closed-form solution:

$$W_{(\pm k)}(\rho) = \frac{(\lambda \rho)^{\pm \alpha_k + \frac{1}{2}}\, {}_2F_1(\pm \alpha_k + \sigma k + \frac{1}{2}, \pm \alpha_k - \sigma k + \frac{1}{2}; 1 \pm 2\alpha_k; \lambda \rho)}{-\log(1 - \lambda \rho)}; \tag{A.15}$$

- the grading $g(\rho) = (\lambda \rho)^{-\frac{1}{2}}(1 - \lambda \rho)^{\frac{1}{2}} \arcsin^2(\sqrt{\lambda \rho})$, yields the closed-form solution:

$$W_{(\pm k)}(\rho) = \frac{(\lambda \rho)^{\pm \alpha_k + \frac{1}{4}}\, {}_2F_1(\pm \alpha_k + \sigma k + \frac{1}{4}, \pm \alpha_k - \sigma k + \frac{1}{4}; 1 \pm 2\alpha_k; \lambda \rho)}{\arcsin(\sqrt{\lambda \rho})}. \tag{A.16}$$

References

Abramowitz, M., Stegun, I.A., 1965. Handbook of Mathematical Functions with Formulas, Graphs and Tables. Dover, New York.

Andrianov, I.V., Bolshakov, V.I., Danishevs'kyy, V.V., Weichert, D., 2007. Asymptotic simulation of imperfect bonding in periodic fibre-reinforced composite materials under axial shear. Int. J. Mech. Sci. 49, 1344–1354.

Andrianov, I.V., Danishevs'kyy, V.V., Kalamkarov, A.L., 2008. Micromechanical analysis of fibre-reinforced composites on account of influence of fiber coatings. Composites: Part B 39, 874–881.

Apostol, T.M., 1997. Modular Functions and Dirichlet Series in Number Theory, secon ed. Springer-Verlag, New York.

Artioli, E., Bisegna, P., Maceri, F., 2010. Effective longitudinal shear moduli of periodic fibre-reinforced composites with radially-graded fibres. Int. J. Solids Struct. 47, 383–397.

Bensoussan, A., Lions, J.-L., Papanicolau, G., 1978. Asymptotic Analysis for Periodic Structures. North-Holland, Amsterdam.

Bertrand, P., Vidal-Setif, M.H., Mevrel, R., 1995. LPCVD pyrocarbon coating on unidirectional carbon fiber yarns: an efficient interphase for aluminium matrix composites. J. Phys. IV 5, C5-769–C5-776.

Bigoni, D., Serkov, S.K., Valentini, M., Movchan, A.B., 1998. Asymptotic models of dilute composites with imperfectly bonded inclusions. Int. J. Solids Struct. 35 (24), 3239–3258.

Bisegna, P., Caselli, F., 2008. A simple formula for the effective complex conductivity of periodic fibrous composites with interfacial impedance and applications to biological tissues. J. Phys. D: Appl. Phys. 41, 115506 (13pp.).
Bonnet, G., 2007. Effective properties of elastic periodic composite media with fibers. J. Mech. Phys. Solids 55, 881–899.
Brendel, A., Paffenholz, V., Köck, T., Bolt, H., 2009. Mechanical properties of sic long fibre reinforced copper. J. Nucl. Mater. 386–388, 837–840.
Brendel, A., Popescu, C., Schurmann, H., Bolt, H., 2005. Interface modification of sic-fibre/copper matrix composites by applying a titanium interlayer. Surf. Coat. Technol. 200, 161–164.
Buryachenko, V., 2007. Micromechanics of Heterogeneous Materials. Springer, Berlin.
Chen, T., Kuo, H.-Y., 2005. Transport properties of composites consisting of periodic arrays of exponentially graded cylinders with cylindrically orthotropic materials. J. Appl. Phys. 98, 033716.
COMSOL AB, 2008. Comsol Multiphysics® User's Guide (version 3.5). <http://www.comsol.com/>.
Du, J., Höschen, T., Rasinski, T., You, J.-H., 2010. Interfacial fracture behavior of tungsten wire/tungsten matrix composites with copper-coated interfaces. Mater. Sci. Eng. A 527, 1623–1629.
Friebel, C., Doghri, I., Legat, V., 2006. General mean-field homogenization schemes for viscoelastic composites containing multiple phases of coated inclusions. Int. J. Solids Struct. 43, 2513–2541.
Hashemi, R., Kargarnovin, M.H., 2011. Overall electroelastic moduli of particulate piezocomposites with non-dilute BCC microstructure. Int. J. Mech. Sci. 53 (9), 777–785.
Hashin, Z., 1991. The spherical inclusion with imperfect interface. J. Appl. Mech. 58, 444–449.
Helsing, J., 1995. An integral equation method for elastostatics of periodic composites. J. Mech. Phys. Solids 43, 815–828.
Iwakuma, T., Nemat-Nasser, S., 1983. Composites with periodic microstructure. Comput. Struct. 16, 13–19.
Jiang, C.P., Xu, Y.L., Cheung, Y.K., Lo, S.H., 2004. A rigorous analytical method for doubly periodic cylindrical inclusions under longitudinal shear and its applications. Mech. Mater. 36, 225–237.
Jones, R.M., 1999. Mechanics of Composite Materials. Taylor & Francis, Philadelphia.
Kalamkarov, A.L., 1992. Composite and Reinforced Elements of Construction. Wiley, Chichester, NY.
Kantor, Y., Bergman, D.J., 1982. Elastostatic resonances – a new approach to the calculation of the effective elastic constants of composites. J. Mech. Phys. Solids 30, 355–376.
Kushch, V.I., Sevostianov, I., Mishnaevsky Jr, L., 2008. Stress concentration and effective stiffness of aligned fiber reinforced composite with anisotropic constituents. Int. J. Solids Struct. 45, 5103–5117.
Lene, F., Leguillon, D., 1982. Homogenized constitutive law for a partially cohesive composite material. Int. J. Solids Struct. 18, 443–458.
Rayleigh, Lord, 1892. On the influence of obstacles arranged in rectangular order upon the properties of a medium. Philos. Mag. 34, 481–502.
Meguid, S.A., Kalamkarov, A.L., 1994. Asymptotic homogenization of elastic composite with a regular structure. Int. J. Solids Struct. 31 (3), 303–316.
Michel, J.C., Moulinec, H., Suquet, P., 1999. Effective properties of composite materials with periodic microstructure: a computational approach. Comput. Meth. Appl. Mech. Eng. 172, 109–143.
Milton, G.W., 2004. The theory of composites. Cambridge Monographs on Applied and Computational Mathematics, vol. 6. Cambridge University Press, Cambridge.
Mura, T., 1987. Micromechanics of defects in solids. Mechanics of Elastic and Inelastic Solids,, Martinus Nijhoff Publishers, Dordrecht.
Nicorovici, N.A., McPhedran, R.C., Milton, G.W., 1993. Transport properties of a three-phase composite material: the square array of coated cylinders. Proc. R. Soc. Lond. A 442, 599–620.
Nose, M., Kawabata, T., Watanuki, T., Ueda, S., Fujii, K., Matsuda, K., Ikeno, S., 2011. Mechanical properties and oxidation resistance of craln/bn nanocomposite coatings prepared by reactive dc and rf cosputtering. Surf. Coat. Technol. 205, S33–S37.
Parnell, W.J., Abrahams, I.D., 2006. Dynamic homogenization in periodic fibre reinforced media. Quasi-static limit for SH waves. Wave Motion 43, 474–498.
Perrins, W.T., McKenzie, D.R., McPhedran, R.C., 1979. Transport properties of regular arrays of cylinders. Proc. R. Soc. Lond. A 369, 207–225.
Rodríguez-Ramos, R., Sabina, F.J., Guinovart-Díaz, R., Bravo-Castillero, J., 2001. Closed-form expressions for the effective coefficients of a fiber-reinforced composite with transversely isotropic constituents – I. Elastic and square symmetry. Mech. Mater. 33, 223–235.
Sanchez-Palencia, E., 1980. Non-Homogeneous Media and Vibration Theory. Lecture Notes in Physics. Springer, Berlin.
Sevostianov, I., Rodríguez-Ramos, R., Guinovart-Díaz, R., Bravo-Castillero, J., Sabina, F.J., 2012. Connections between different models describing imperfect interfaces in periodic fiber-reinforced composites. Int. J. Solids Struct. 49, 1518–1525.
Wang, J., Crouch, S.L., Mogilevskaya, S.G., 2006. Numerical modeling of the elastic behavior of fiber-reinforced composites with inhomogeneous interphases. Compos. Sci. Technol. 66 (1), 1–18.
Whittaker, E.T., Watson, G.N., 1927. A Course of Modern Analysis. Cambridge University Press, Cambridge.
Xun, F., Gengkai, H., Huang, Z., 2004. Effective in plane moduli of composites with a micropolar matrix and coated fibers. Int. J. Solids Struct. 41, 247–265.
Zhang, L., Shi, N., Gong, J., Sun, C., 2011. Preparation of sic fiber reinforced nickel matrix composite. J. Mater. Sci. Technol. 28 (3), 234–240.